33rd Annual International Conference of the IEEE EMBS
Boston, Massachusetts USA, August 30 - September 3, 2011

Accurate positioning of magnetic microparticles beyond the spatial resolution of clinical MRI scanners using susceptibility artifacts

N. Olamaei, *Student Member, IEEE,* F. Cheriet, *Senior Member, IEEE*, S. Martel, *Senior Member, IEEE,*

***Abstract*— Susceptibility-based negative contrast in magnetic resonance imaging (MRI) provides a mean to visualize magnetic microparticles. In the presence of a number of micropaticles in the field of view (FOV), the shape of the artifact is affected by the dipole-dipole interaction between the particles. Due to the limited spatial resolution of the clinical MR scanners, the exact positioning of the particles in MR images is not possible. However, the shape of the artifact can shed light on how the particles are distributed within the FOV. In this work, a simulation model and in-vitro experiments were used to study the shape and the amount of the susceptibility artifact for various spacing and angulations between the microparticles. The results showed that for a pair of identical particles with a diameter of D, the signal loss starts to change when particles are separated ~15×D and they become fully distinguishable when their distance reaches ~ 40×D.**

I. Introduction

MRI has a wide range of applications in visualization of magnetic microparticles e.g. angiography using contrast agents, molecular and cellular imaging [1-3] and real-time drug delivery to the tumor sites [4]. Compared to nanofabricated agents, micrometer-sized agents can benefit from higher magnetic moments which increase their ability to produce MRI-visible artifacts. Based on equivalent amount of magnetic material, micrometer-sized particles have up to 50% higher relaxivity [5]. In equal iron contents, they have also shown to produce a larger hypointense signal in T_2^*-weighted images [6].

Real-time drug delivery technique to the tumor sites is based on therapeutic magnetic micro carriers (TMMC) which can be steered and tracked using an upgraded magnetic resonance imaging (MRI) system. TMMC is an MR navigable microparticle with a diameter of ~50 µm loaded with ferromagnetic and therapeutic particles and designed for target embolization [7]. The aim of the targeting is to focus TMMCs at the entry of the arteriocapillar network through embolization (Fig. 1). High resolution ferromagnetic microparticle sensitive $T2^*$-weighted MR scans are performed prior and subsequent to the injection of TMMCs to record the spatial distribution of the embolizing microcarriers. The distribution of the TMMCs can display a map of the local microvascular bifurcations.

Pre-clinical high field scanners facilitate obtaining the desirable resolution for resolving microstructures in animal models [8-10]. However, microstructure systems cannot be imaged using current clinical imaging modalities. In [11], we showed that the susceptibility-based contrast provides a mean to detect ferromagnetic microparticles as small as 15 µm in diameter in the images of a clinical MR scanner (Fig. 1). The results suggested the possibility of microstructures visualization through susceptibility artifact using magnetic agents. However, the presence of numerous microparticles in the region of interest (ROI) affects the susceptibility artifact by the dipole-dipole interactions. Hence, the shape of the artifact becomes dependent on the distribution of the microparticles and their spacing. This makes detection and positioning of the individual microparticles challenging.

In this work, we studied the shape of the susceptibility artifact generated by ferromagnetic cores distributed in an unknown fashion over the field of view. The result was used to determine the position of the microparticles relative to each other.

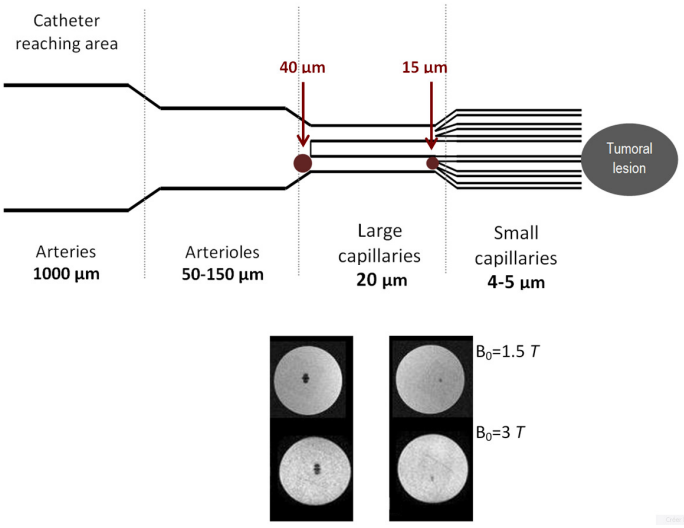

Fig. 1 Experimental coronal images of two stainless steel microparticles measured 40µm and 15 µm in diameter, using external field strength of 3T and 1.5T.

Manuscript received April 15, 2011. This work was supported in part by the Fond Québecois de la Recherche sur la Nature et les Technologies (FQRNT) and grants from the National Sciences and Engineering Research Council of Canada (NSERC).

Nina Olamaei is with the École Polytechnique Montréal, QC, H3C 3A7, Canada (e-mail: nina.olamaei@polymtl.ca).

Farida Cheriet is with the Sainte-Justine Hospital Research Center and École Polytechnique Montréal, Montreal, QC, H3C 3A7 Canada, (e-mail: farida.cheriet@polymtl.ca).

Sylvain Martel (corresponding author) is with the NanoRobotics Laboratory, Department of Computer and Software Engineering, and the Institute of Biomedical Engineering, École Polytechnique Montréal, Montreal, QC, H3C 3A7, Canada, (e-mail: sylvain.martel@polymtl.ca).

II. Materials and Methods

A. Distorted patterns of ferromagnetic microparticles

Ferromagnetic materials induce a distorted region in MR images due to the field inhomogeneties caused by their high magnetic susceptibility. The field induced by sphere magnetic particles can be approximated by that of a dipole.

The susceptibility difference is the source of two types of artifact in MR images; geometrical distortion and echo shifting. Geometrical distortion is any misregistration of spin positions caused by field variations during frequency encoding [12-14]. If G' represents the static background gradient created by field inhomogeneties, spins residing at position x will be mapped to position x':

$$x' = x\left(1 + \frac{G'_x}{G_x}\right) \tag{1}$$

Background gradient along the phase encoding direction (perpendicular to the readout direction) imposes a distortion on the voxel shape. Image distortion is reflected on both the gradient echo sequence (GE) and the spin echo sequence (SE). On the other hand, due to the 180° refocusing pulse of the SE sequences, the echo shifting effect only appears in GE images. The influence of a position dependent phase term is added to that of the unusual scaling of the k-space variable (as in SE) to determine the position of the spins:

$$\varphi(x) = -2\pi\gamma G'_x x TE \tag{2}$$

When the phase dispersion is a nonzero positive integer multiple of 2π, the voxel signal vanishes completely. Therefore, echo shifting creates a signal loss in MR images. GE images are affected by both forms of artifacts; however echo shifting has a dominant effect on the geometrical distortion in GE scans. In [15], two different image simulations have been compared: a) based on geometrical distortion and phase dispersion and b) based on phase dispersion only. Significant deviations have been observed in the results obtained for high resolution images (< 100 μm) produced in high field MRI scanners. Nevertheless, for image resolutions of > 200 μm (clinical MR scanners) the difference has not been significant.

Total signal loss in GE imaging is expected to be independent of the in-plane resolution and the geometrical distortion [16]. Moreover, the position of the artifact is expected to reflect the exact position of the microparticle.
For intravoxel dephasing, the measured signal within the volume of interest in GE imaging and with a homogeneous spin density (ρ) is described by:

$$S(t) = \int_v \rho \exp(-i\varphi(\vec{r},t))dv \tag{3}$$

$$\varphi(t) = \gamma B_z(\vec{r})TE, \tag{4}$$

where φ is the phase dispersion across the voxel, TE is the echo time and γ is the gyromagnetic ratio for protons. The field distribution induced by ferromagnetic objects at position $\vec{r}$ varies as [12]:

$$\Delta B_z(\vec{r}) = \sum_{i=1}^{N} \frac{\mu_0}{4\pi}\left(3\left(\frac{(\vec{m}.\vec{r}_i)\vec{r}_i}{r_i^5} - \frac{\vec{m}}{r_i^3}\right)\right) \text{ with } \vec{m} = \frac{1}{6}\pi D^3 \vec{M}_{sat}, \tag{5}$$

where $\vec{m}$ is the net dipole moment, N is the number of the particles within the field of view (FOV), D is the diameter of the particles and $\vec{M}_{sat}$ is the magnetization saturation of the particles. The normalized signal is given by:

$$\frac{s}{s_0} = \int_v \rho \exp(-i\Delta B_z(\vec{r})TE)dv \cdot \tag{6}$$

B. Simulation study

The susceptibility artifact of particles was simulated using MATLAB® programming language and based on the intravoxel dephasing caused by the phase accumulation at the TE in the GE scan (see equation (6)). The area of the S_{loss} was calculated by summing the in plane signal loss over the region of interest. Different distances and angles between microparticles were simulated to study the pattern of the artifacts and the minimum distance required to see them distinguishably. The images were evaluated for a coronal plane with a slice thickness of 3.5 mm and a pixel spacing of 0.5 mm. It was assumed that the microparticles are saturated at the magnetic field strength of 1.5 T.

C. In-vitro study

Phantom experiments were carried out using chrome-steel microspheres (Salem specialty Ball Co., Inc.) measured 0.4 mm and 0.8 mm in diameter and a saturation magnetization of ~1.3×10^6 A/m. Pairs of particles at distances set to different multiples of their diameters (15×D, 30×D, 40×D and 80×D) were fixed on plastic plates. Each pair was suspended in the middle of a solution made up of gelatin and Sodium Chloride to mimic the human body relaxation times. Imaging was performed using 1.5 T (Magnetom Siemens) MRI systems. Images were acquired with the standard 8 channel head coil and the following identical GE parameters: FOV = 100 mm × 160 mm, TR = 500 ms, imaging matrix = 256, slice thickness = 3.5 mm, flip angle = 25°, pixel spacing = 0.5 mm, TE = 10 ms.

III. Results

Figure 2 presents signal intensity of the simulated GE images for different distances between particles, varied from 5×D to 120×D, and for particles of different diameters (20 μm, 50 μm, 100 μm and 200 μm). Signal intensity remains about the same for the distances less than 15×D. From 15×D to 40×D the signal loss grows in size as the form of the artifact starts to change. At the distance of 40×D and more the artifacts get separated and as such the signal intensity remains constant. The signal loss was calculated for an in-plane resolution of 0.5×0.5 mm^2 which is a typical resolution of a clinical MR scanner. However, the signal loss calculated for particles of different diameters and spacing showed to be independent of the image in-plane resolution (results are not shown here). In figure 3, particles (D=40 μm) are distanced

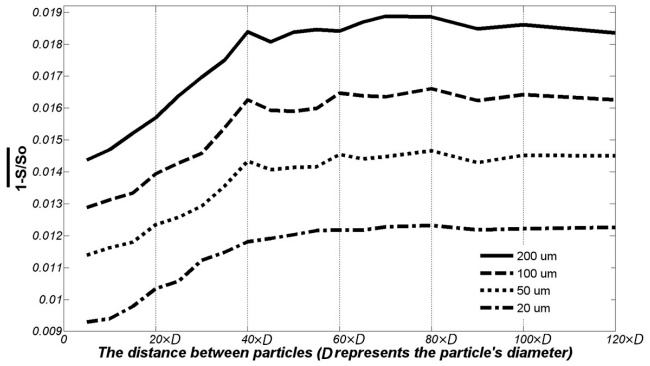

Fig. 2. Simulated GE signal intensity as a function of the distance between the particles on the coronal plane with the following scan parameters: B_0=1.5T, in-plane resolution = 0.5×0.5 mm^2 and TE=10ms. The distance is labeled by multiples of the particles' diameter (*D*). Curve labels indicate the diameter of the particles in micrometer.

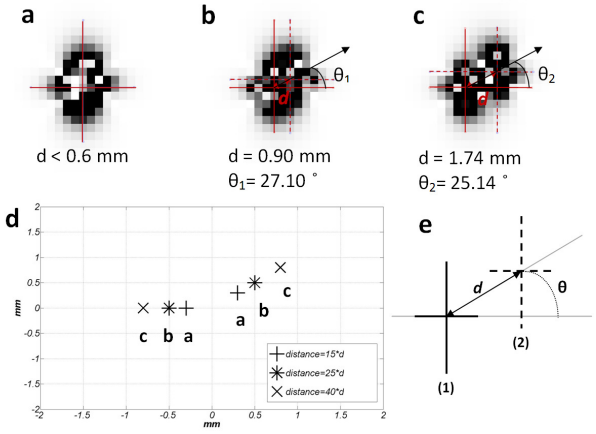

Fig. 3. GE simulated signal of the micropaticles measured 40 µm in diameter with the following scan parameters: B_0=1.5T, TE=10ms, in-plane resolution = 0.4×0.4 mm^2 distances at 15×D (a), 25×D (b) and 40×D (c). Each pair of the particles were distanced and angulated according to the plot d. The centers of the artifacts (1) and (2) were used to calculate the distance and the angle between the particles (e).

at 15×D, 25×D and 40×D along the *x*-axis and are placed in an angular position (Fig. 3d). Simulated GE images with an in-plane resolution of 0.5×0.5 mm^2 and a field of view of 2.0×2.0 cm^2 can be used to estimate the distance and the angle between the particle pairs. The position of the artifact in GE scans is expected to reflect the exact position of the microparticle. Therefore, positions of the particles were determined by finding the center of artifacts. The artifact has the shape of a four leaf-clover with two axes of symmetry. The center of the artifact is the point where the axes intersect (Fig. 3a). Coordinates of the centers were used to calculate the distance and the angle between the particles (Fig. 3e). At the distance of 15×D the particles are not distinguishable as the artifacts are almost completely superimposed (figure 3a). At 25×D, the signal represents two artifacts which are partly superimposed. However, centers of the artifacts can be determined (Fig. 3b). The distance and the angle between the particles were measured as 0.9 mm and 27.1˚ whereas the real values were 1.1 mm and 26.56˚. These parameters were calculated as 1.74 mm and 25.14˚ at the distance of 40×D while the real values were 1.78 mm and 26.98˚. Figure 4 shows a distribution of the particles (D = 20µm) with different distances and angulations (part *c*). Simulated GE signals are shown for an image in-plane resolution of 0.2×0.2 mm^2 and 0.5×0.5 mm^2. The former is a typical resolution of high field MR scanners (7 T) and the latter is a typical resolution of clinical MR scanners (1.5 T and 3 T).

In [11], we validated the simulation model using a statistical analysis and the results showed that there was no significant difference between the MRI images of magnetic microparticles of various diameters and the images produced by the simulation model (p = 0.075). In-vitro experiments were performed to validate the method proposed for positioning the magnetic microparticles and also the simulation results. In order to accurately manipulate the distance between the particles, those at a millimeter-scale

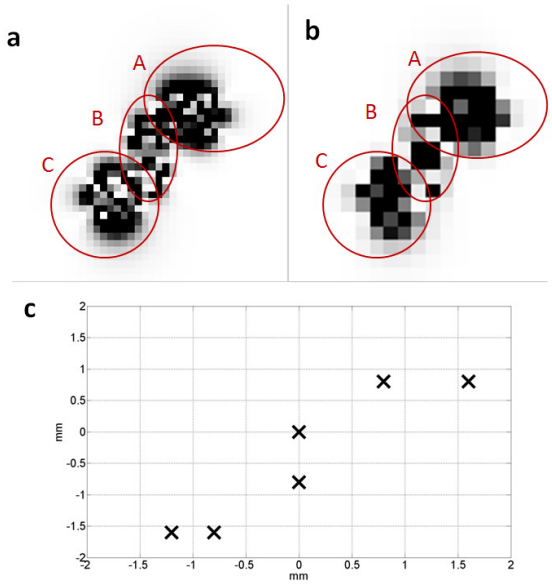

Fig. 4. GE simulated signal of the micropaticles measured 20 µm in diameter using the following scan parameters: B_0=1.5T, TE=10ms, in-plane resolution = 0.2×0.2 mm^2 (*a*) and 0.5×0.5 mm^2 (*b*). The particles are distributed according to the plot *c*. Circled regions show particle pairs with different spacing. Region A presents two particles distanced within 15×D and 40×D. Region B and C present two particles distanced at 40×D and smaller than 15×D, respectively.

(0.4 mm and 0.8 mm) were used. The MR images were compared with the simulated images of the particles of the same diameter.

Figure 5 shows measured and simulated signals of the particle pairs at different distances. At 15×D (Fig. 5b) the form of the artifact remains the same as that of a single artifact, while the artifact increases in size. At 30×D the artifact changes in form and it grows in size (Fig. 5c). At 40×D the artifact represents the two particles clearly (Fig. 5d).

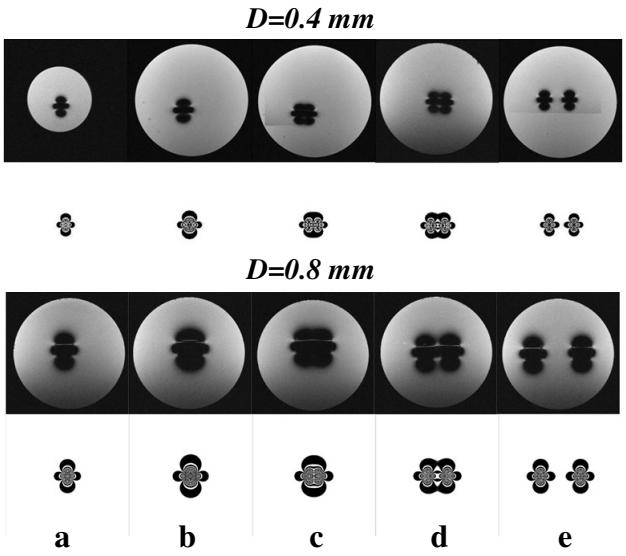

Fig. 5. Experimental (odd rows) and simulated (even rows) coronal images of 0.4 mm and 0.8 mm chrome-steel microspheres; (*a*) a single microparticle and (b) to (e) pairs distanced at 15×D, 30×D, 40×D and 80×D respectively. Identical scan parameters were B_0=1.5T, in plane resolution 0.6×0.6 mm^2 and TE=10 ms.

Using centers of the artifacts, the distance between particles were measured in both the MR images and the simulated images. The results were compared using a paired Student's *t*-test with statistical significance defined for probability values less than 5%. No significant difference between the two observations were found ($p = 0.16$).

IV. Discussion and Conclusion

A technique capable of positioning magnetic microparticles can be applied into many research areas dealing with visualization of microstructures such as cellular and microvascular imaging. Using a clinical MRI system, a single 15 μm microsphere is detectable in gradient-echo scans. Particles at this dimension can easily reach the capillary system and be used as steerable and trackable agents. Due to the limited spatial resolution of clinical MRI systems, the exact positioning of the individual particles in MR images of a clinical scanner is not possible. However, the shape of the signal loss in GE images can shed light onto the local distribution of the particles in a region of interest within the human body. Assuming that the injected microparticles have identical diameters and saturation magnetization values, the following statements can be concluded from the results obtained from the current work:

i) If the distance is < 15×D, the artifacts generated by the individual particles are almost entirely superimposed and the shape of the signal loss is similar to that of a single particle. However, the amount of the signal loss can represent the number of the particles,

ii) If the distance is > 15×D and < 40×D, the artifacts are partially superimposed. The distance and the angle between the particles can be calculated by locating their centers. Nevertheless, artifacts being superposed, their centers cannot be accurately positioned,

iii) If the distance is > 40×D, the artifacts are separated. The distance and the angle between the particles can be calculated more precisely.

The obtained cutoff values (15×D and 40×D) were shown to be independent of the diameter of the particles and the resolution of the image. However, image analysis in finding the center of the artifacts is more accurate at higher resolutions (Fig. 4). As a support measure, a simulation model was used to study the shape of the susceptibility artifact in MR images in the presence of a number of magnetic microparicles. The results showed that the accuracy of the estimated position of the particles highly depends on particles' spacing and angulation.

References

[1] J. W. Bulte and D. L. Kraitchman, "Iron oxide MR contrast agents for molecular and cellular imaging," *NMR Biomed,* vol. 17, pp. 484-99, Nov 2004.

[2] E. M. Shapiro, *et al.*, "Sizing it up: Cellular MRI using micron-sized iron oxide particles," *Magnetic Resonance in Medicine,* vol. 53, pp. 329-338, Feb 2005.

[3] E. M. Shapiro, *et al.*, "MRI detection of single particles for cellular imaging," *Proceedings of the National Academy of Sciences of the United States of America,* vol. 101, pp. 10901-10906, Jul 27 2004.

[4] P. Pouponneau, *et al.*, "Magnetic nanoparticles encapsulated into biodegradable microparticles steered with an upgraded magnetic resonance imaging system for tumor chemoembolization," *Biomaterials,* vol. 30, pp. 6327-6332, Nov 2009.

[5] K. A. Hinds, *et al.*, "Highly efficient endosomal labeling of progenitor and stem cells with large magnetic particles allows magnetic resonance imaging of single cells," *Blood,* vol. 102, pp. 867-872, Aug 1 2003.

[6] C. Luna, *et al.*, "Multidomain to single-domain transition for uniform Co80Ni20 nanoparticles," *Nanotechnology,* vol. 14, pp. 268-272, Feb 2003.

[7] P. Pouponneau, *et al.*, "Co-encapsulation of magnetic nanoparticles and doxorubicin into biodegradable microcarriers for deep tissue targeting by vascular MRI navigation," *Biomaterials,* vol. 32, pp. 3481-6, May 2011.

[8] G. A. Christoforidis, *et al.*, "Visualization of microvascularity in glioblastoma multiforme with 8-T high-spatial-resolution MR imaging," *AJNR Am J Neuroradiol,* vol. 23, pp. 1553-6, Oct 2002.

[9] R. A. Dashner, *et al.*, "Limits of 8-Tesla magnetic resonance imaging spatial resolution of the deoxygenated cerebral microvasculature," *Journal of Magnetic Resonance Imaging,* vol. 19, pp. 303-307, Mar 2004.

[10] S. Foxley, *et al.*, "Sensitivity to Tumor Microvasculature Without Contrast Agents in High Spectral and Spatial Resolution MR Images," *Magnetic Resonance in Medicine,* vol. 61, pp. 291-298, Feb 2009.

[11] N. Olamaei, *et al.*, "MRI visualization of a single 15 microm navigable imaging agent and future microrobot," *Conf Proc IEEE Eng Med Biol Soc,* vol. 2010, pp. 4355-8, 2010.

[12] E. M. Haacke, *Magnetic resonance imaging : physical principles and sequence design*. New York: Wiley, 1999.

[13] S. Posse and W. P. Aue, "Susceptibility Artifacts in Spin-Echo and Gradient-Echo Imaging," *Journal of Magnetic Resonance,* vol. 88, pp. 473-492, Jul 1990.

[14] C. J. G. Bakker, *et al.*, "Simulation of Susceptibility Artifacts in 2d and 3d Fourier-Transform Spin-Echo and Gradient-Echo Magnetic-Resonance-Imaging," *Magnetic Resonance Imaging,* vol. 12, pp. 767-774, 1994.

[15] G. Zabow, *et al.*, "Microfabricated high-moment micrometer-sized MRI contrast agents," *Magn Reson Med,* Oct 6 2010.

[16] C. Bos, *et al.*, "On the artifact of a subvoxel susceptibility deviation in spoiled gradient-echo imaging," *Magn Reson Med,* vol. 50, pp. 400-4, Aug 2003.